Modelling self- and shear-noise mechanisms in inhomogeneous, anisotropic turbulence

P. Jordan*, Y. Gervais

Laboratoire d'Etudes Aérodynamiques, CNRS UMR 6609, Université de Poitiers, Bâtiment K, Avenue du Recteur Pineau, 86022 Poitiers, France

Abstract

A statistical jet noise model which includes the effects of mixing layer inhomogeneity and anisotropy is presented. The model adapts the spatial and temporal correlation function models frequently used in jet noise prediction, so that the axial, radial and lateral integral space and time scales are included to model flow anisotropy, the spatial structure of the Reynolds stress field being used to account for flow inhomogeneity. These flow properties have been estimated from single and multi-point LDV measurements performed in the mixing layer of an isothermal jet with a Mach number of 0.75. The model is used to assess acoustic contributions from the constituent self- and shear-noise quadrupoles. Results highlight the very different nature of the self- and shear-noise source mechanisms and identify those aspects of the flow structure on which their sound production efficiency depends. The dependence of the shear noise on the radial distance over which the turbulence is correlated illustrates how an isotropic model will overestimate this term. The model demonstrates how sound generation is largely dominated by axially aligned longitudinal quadrupoles and shows the self-noise mechanisms to dominate the shear by a factor of about 2.5 when the flow is anisotropic. A moving-axis temporal correlation model is used to derive expressions for the acoustic spectra of the component quadrupoles, the inclusion of whose time scales allows the temporal manifestation of the flow anisotropy to be modelled. Model predictions are compared with acoustic measurements performed on the same jet and good agreement is found for emission angles between $30°$ and $100°$.
© 2003 Elsevier Ltd. All rights reserved.

*Corresponding author.

E-mail address: peter.jordan@lea.univ-poitiers.fr (P. Jordan).

1. Introduction

Sound generation by turbulent fluid motion involves a conversion of the energy associated with rotational hydrodynamic motion to the energy of irrotational propagative motion. However, the precise nature of the mechanisms by which a jet flow achieves this conversion remains unclear. Lighthill [1] made an important step towards understanding these mechanisms in formally expressing the acoustic field generated by a jet flow in terms of its turbulence dynamics. In relating the acoustic field to the spatiotemporal correlation of the turbulence Reynolds stress tensor, he showed how the latter could be viewed as a volume distribution of quadrupole acoustic source mechanisms. He thus made it clear, that if the nature of the energy-conversion mechanisms alluded to above are to be understood, the structure of the Reynolds stress field comprising a jet flow must be investigated, and those aspects most relevant to the generation of sound assessed.

A second decisive initiative was Ribner's decomposition of the turbulence velocity vector into mean and fluctuating parts [2]. This allowed the source mechanisms comprising the spatiotemporal Reynolds stress correlation to be separated into two distinct components, those arising from the turbulence alone, whose contribution to the acoustic field was labelled *self-noise*, and those resulting from an interaction of the turbulence with the mean flow, the acoustic field of which is known as *shear noise*. Ribner's analysis went still further in allowing the self- and shear-noise components of the sound generation process to be expressed in terms of their constituent mechanisms. Described using a Cartesian system these constituents include a mechanism involving axial motion only (axially aligned longitudinal quadrupoles), one involving radial motion only (radially aligned longitudinal quadrupoles) and one in which both axial and radial motions contribute (lateral quadrupole). Ribner assumed furthermore a spatiotemporal correlation function separable into independent functions of space and time. Individual contributions from each of the quadrupoles are then found to comprise a number of independent factors: (1) the energy of the turbulence velocity components which appear in the quadrupole correlation, (2) a directional factor depending on the particular form of the quadrupole (lateral, longitudinal or radial), (3) in the case of shear noise the velocity gradient, (4) the integral of the spatial part of the correlation function over a correlation volume and (5) the fourth time derivative of the temporal component of the correlation function. By means of single and two-point turbulence velocity measurements it is possible to obtain the quantities necessary for modelling of these flow characteristics, thus providing an estimate of the quadrupole field structure, whence using Lighthill's formalism the spatiotemporal character of the acoustic field can be evaluated.

Ribner's work is the principal basis of many statistical jet noise models (see Ref. [3] for example). However a recurrent difficulty is encountered in the assumption of flow isotropy and homogeneity, whence the use of a single characteristic length scale is justified to describe the spatial decay of the velocity correlation, a single characteristic time scale to describe its temporal decay rate, and a single value of the turbulence intensity to represent the kinetic energy of the flow.

In this work, an approach developed by Devenport et al. [4] to account for the spatial inhomogeneity of the flow is adapted to include anisotropy effects and used thus to derive analytical expressions for the second and fourth order velocity correlation tensors, representative

of the shear- and self-noise mechanisms, respectively. A temporal model is also developed, to evaluate the effects of anisotropy on the spectral character of these mechanisms and their resultant sound field. The approach involves the introduction of both axial and radial length scales, and axial, radial and lateral time scales for the various self- and shear-noise quadrupole components. It is found that the self-noise mechanism dominates the shear by a factor of about 2.5 when the flow is considered anisotropic, the axially aligned longitudinal source components being the most significant contributors to the sound field.

2. Theory

The acoustic field generated by a jet flow can be expressed, as shown by Lighthill [1], by

$$P(\mathbf{y}, \theta) = A I_{ijkl}\, dir(ijkl), \tag{1}$$

where

$$A = \rho_o (16\pi^2 c_o^5 x^2 C^5)^{-1},$$

$$I_{ijkl} = \int \frac{\partial^4}{\partial \tau^4} \overline{v_i v_j v_k v_l}\, d^3\mathbf{r},$$

$$dir(ijkl) = (2\pi)^{-1} \int_0^{2\pi} (x_i x_j x_k x_l / x^4)\, d\phi,$$

ρ_o being the ambient air density, c_o the speed of sound, and C the convective amplification factor $(1 - M_c \cos\theta)$. Those components of the velocity correlation tensor which contribute to the sound field are: $ijkl = 1111, 1212, 1122, 2222$.[1] Their directional patterns are

$$dir(1111) = \cos^4\theta,$$

$$dir(1212) = dir(1122) = \tfrac{1}{2}\cos^2\theta \sin^2\theta,$$

$$dir(2222) = \tfrac{3}{8}\sin^4\theta$$

and their respective weight factors (allowing for different permutations of the indices) are 1, 4, 2, and 1.

2.1. The quadrupole correlations

Decomposing the turbulence velocity into mean and fluctuating components

$$v_i = U\delta_{i1} + u_i, \tag{2}$$

where U is the local mean velocity, and u_i the fluctuating component (primed variables correspond to a second spatial location), shows the quadruple velocity correlations contributing

---

[1] Only a two-dimensional slice through the jet is considered, such that the azimuthal direction is ignored (i.e., the indices *ijkl* take on values of 1 or 2).

to the generation of sound to be

$$
\begin{aligned}
R_{1111} &= \overline{u_1^2 u_1'^2} + 4UU'\overline{u_1 u_1'}, \\
R_{1212,2121,1221,2112} &= \overline{u_1 u_2 u_1' u_2'} + UU'\overline{u_2 u_2'}, \\
R_{1122} &= 2\overline{u_1^2 u_2'^2}, \\
R_{2222} &= \overline{u_2^2 u_2'^2}.
\end{aligned}
\tag{3}
$$

The acoustic field is given by

$$
\begin{aligned}
P(\mathbf{y}, \theta) = {}& A\cos^4\theta \int \frac{\partial^4}{\partial\tau^4} R_{1111}\, \mathrm{d}^3\mathbf{r} \\
&+ 4(1/2)A\cos^2\theta\sin^2\theta \int \frac{\partial^4}{\partial\tau^4} R_{1212}\, \mathrm{d}^3\mathbf{r} \\
&+ 2(1/2)A\cos^2\theta\sin^2\theta \int \frac{\partial^4}{\partial\tau^4} R_{1122}\, \mathrm{d}^3\mathbf{r} \\
&+ (3/8)A\sin^4\theta \int \frac{\partial^4}{\partial\tau^4} R_{2222}\, \mathrm{d}^3\mathbf{r}
\end{aligned}
\tag{4}
$$

and this can be separated into contributions from self- and shear-noise mechanisms, expressed, respectively, as

$$
\begin{aligned}
P_{SE}(\mathbf{y}, \theta) = {}& A\cos^4\theta \int \frac{\partial^4}{\partial\tau^4} \overline{u_1^2 u_1'^2}\, \mathrm{d}^2\mathbf{r} \\
&+ 4(1/2)A\cos^2\theta\sin^2\theta \int \frac{\partial^4}{\partial\tau^4} \overline{u_1 u_2 u_1' u_2'}\, \mathrm{d}^2\mathbf{r} \\
&+ 2(1/2)A\cos^2\theta\sin^2\theta \int \frac{\partial^4}{\partial\tau^4} \overline{u_1^2 u_2'^2}\, \mathrm{d}^2\mathbf{r} \\
&+ (3/8)A\sin^4\theta \int \frac{\partial^4}{\partial\tau^4} \overline{u_2^2 u_2'^2}\, \mathrm{d}^2\mathbf{r}
\end{aligned}
\tag{5}
$$

and

$$
\begin{aligned}
P_{SH}(\mathbf{y}, \theta) = {}& 4A\cos^4\theta \int \frac{\partial^4}{\partial\tau^4} UU'\overline{u_1 u_1'}\, \mathrm{d}^2\mathbf{r} \\
&+ 4(1/2)A\cos^2\theta\sin^2\theta \int \frac{\partial^4}{\partial\tau^4} UU'\overline{u_2 u_2'}\, \mathrm{d}^2\mathbf{r}.
\end{aligned}
\tag{6}
$$

The noise generation dynamic is thus described by the spatiotemporal correlation functions, $\overline{u_1 u_1'}$, $\overline{u_2 u_2'}$, $\overline{u_1^2 u_1'^2}$, $\overline{u_2^2 u_2'^2}$, $\overline{u_1^2 u_2'^2}$, and $\overline{u_1 u_2 u_1' u_2'}$. It is these quantities which must be modelled in order to calculate both the relative efficiencies and the spectral character of different source mechanisms.

3. Experiments

Two-component (u and v) single point and mono-component (u) two-point measurements were performed using Laser Doppler Velocimetry (LDV) in the potential core and mixing layer of an isothermal subsonic jet ($M = 0.75$) issuing from a 50 mm nozzle. These experiments were performed at the MARTEL facility of CEAT (Centre d'Études Aérodynamiques et Thermiques), Poitiers, France. The acoustic field was sampled using an arc of microphones at a distance of 30 diameters from and centred on the jet exit. The acoustic and aerodynamic experimental setups are shown in Figs. 1 and 2 and a sample of results from the measurements is shown in Figs. 3–12.

Fig. 3 shows radial profiles of the uu, vv and uv components of the Reynolds stress tensor at $x/D = 5$, demonstrating the spatial inhomogeneity of the flow structure. Figs. 4 and 5 show velocity and Reynolds stress spectra estimated from bi-component single-point LDV measurements performed at the axial positions $x/D = 2.5$ and 5, and at three radial stations, one in the potential core (on the jet axis), one at the edge of the potential core, and one in the centre of the mixing layer (on the jet lip line). Figs. 6–8 show an example of results from the two-point LDV
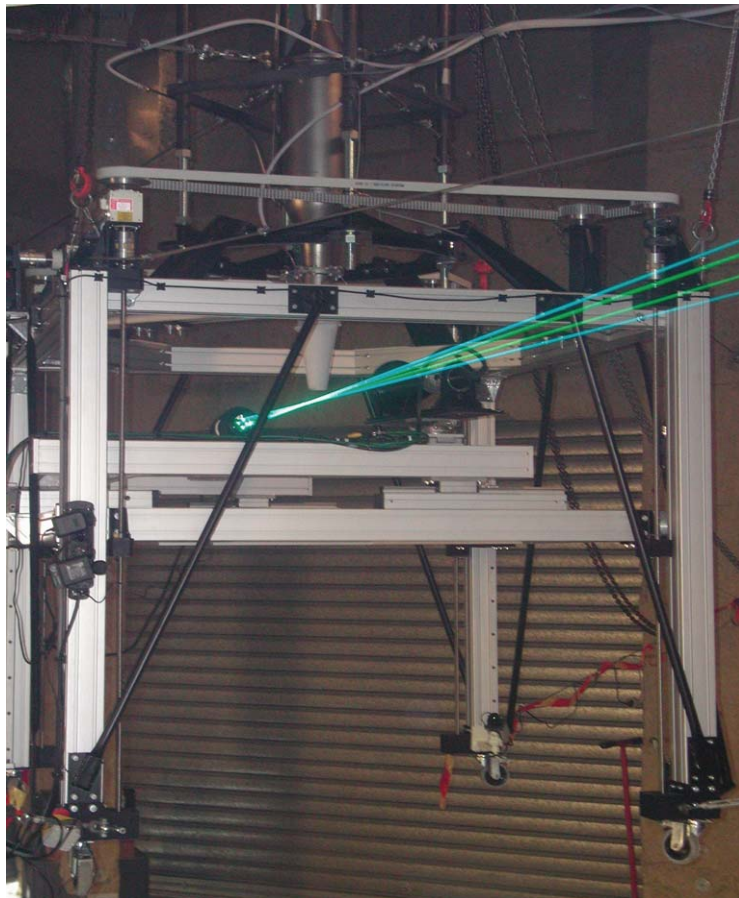

Fig. 1. Bi-component, single point LDV measurement setup.
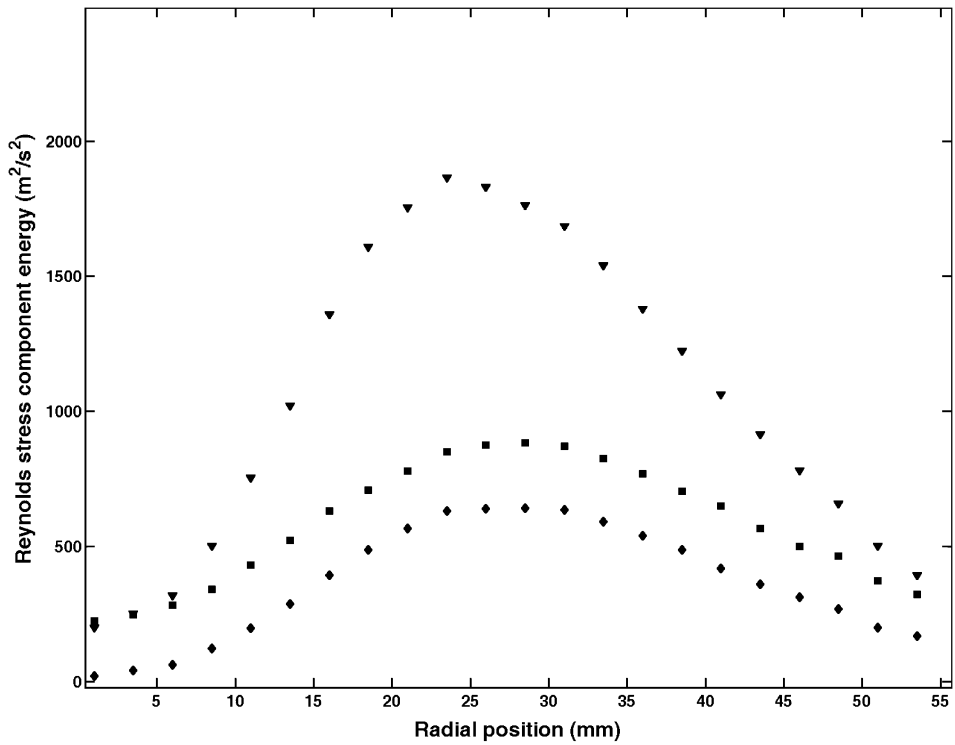
Fig. 2. Acoustic measurement setup.

Fig. 3. Spatial inhomogeneity—radial profiles of Reynolds stress field at $x/D = 5$: ▼, $u'u'$; ▦, $v'v'$; ◆, $u'v'$.
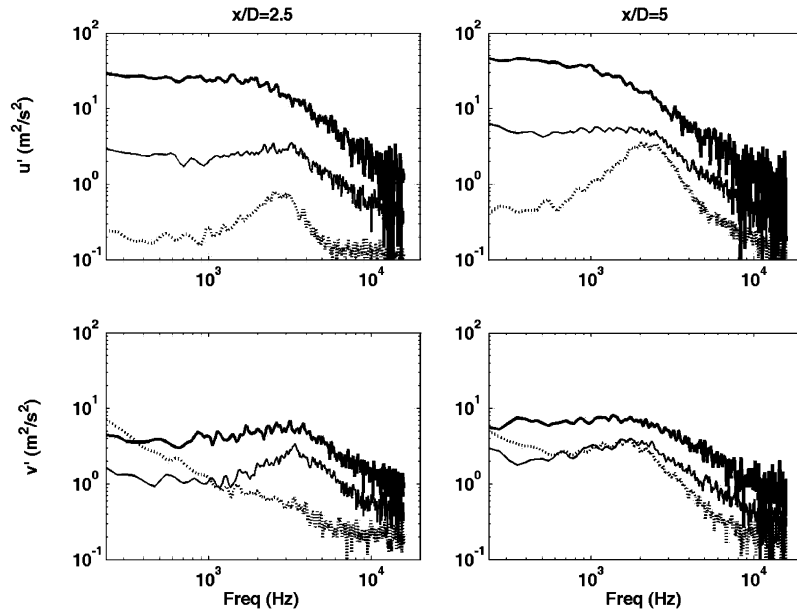
Fig. 4. Velocity spectra: thick solid line—lip line; thin solid line—edge of potential core; dotted line—jet axis.

measurements (longitudinal spatiotemporal correlation of velocity and Reynolds stress fields in the centre of the mixing layer towards the end of the potential core), whence estimates of integral length and time scales (in a moving frame of reference) of the said fields were obtained. Fig. 8 shows the velocity correlation in contour form where the eddy convection velocity is identified by the slope of the line connecting the maxima.

A more comprehensive presentation and analysis of these results will be published in another paper; their purpose here is to demonstrate the inhomogeneous, anisotropic nature of the flow structure, and to include these effects in a statistical jet noise model.

4. Considerations for inhomogeneous, anisotropic turbulence

If the flow structure is considered homogeneous and isotropic the fourth order velocity correlations can be considered to consist of a sum of second order products, the spatial component of which is shown by Batchelor [5] to take the form

$$R_{ij}(\mathbf{r}) = u^2 \left[\left(f(\mathbf{r}) + \frac{r}{2} \frac{df(\mathbf{r})}{dr} \right) \delta_{ij} - \frac{1}{2} \frac{df(\mathbf{r})}{dr} \frac{r_i r_j}{r} \right], \tag{7}$$

where $f(\mathbf{r})$ defines the spatial decay of the velocity correlation (taken by Ribner as $e^{-\pi r^2/L_t^2}$), L_t being a typical turbulence length scale and u a typical *rms* turbulence velocity. Different forms have been proposed for the temporal component of the correlation function, including exponential, Gaussian and hyperbolic functions (see Ribner [2] for a summary of some of these). In all of these functions there appears τ_c, a characteristic time scale, which serves to model the
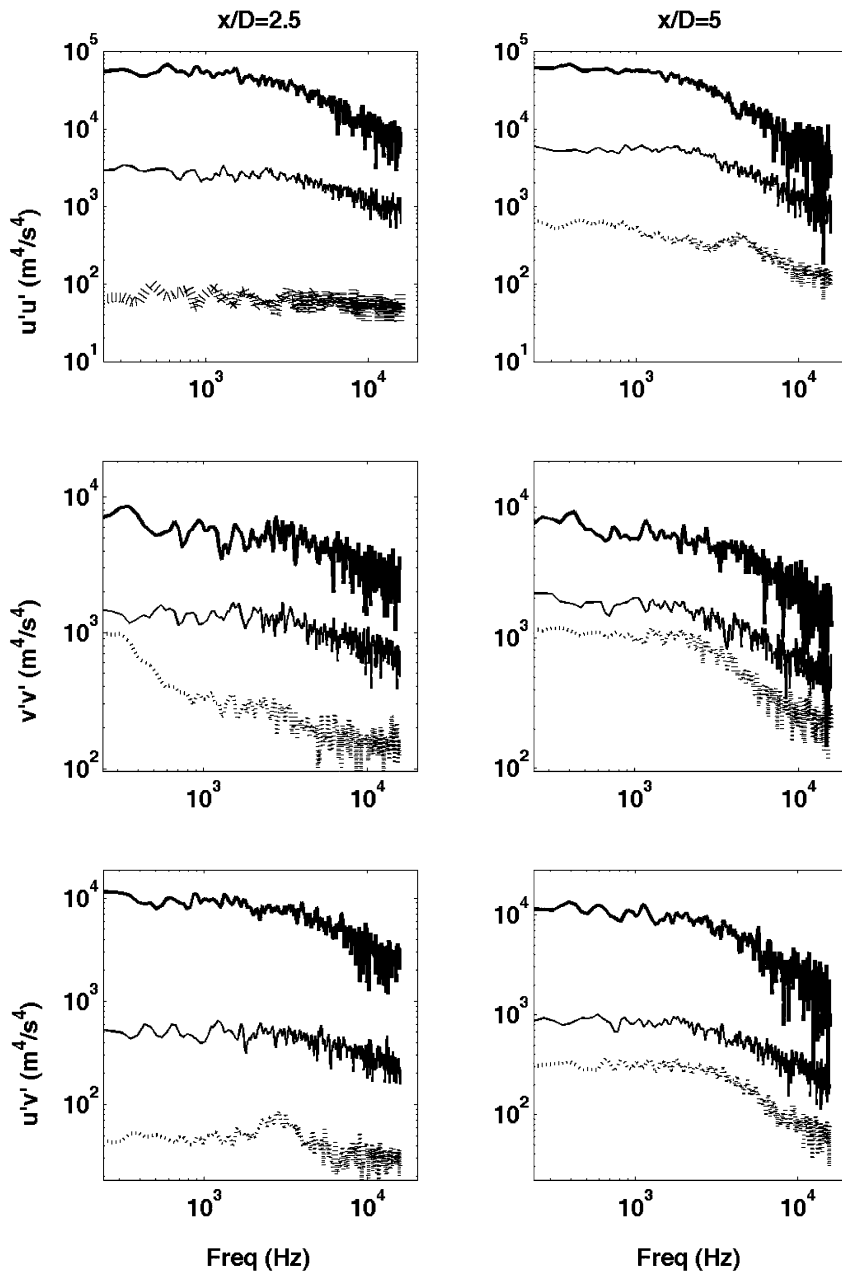
Fig. 5. Reynolds stress spectra: thick solid line—lip line; thin solid line—edge of potential core; dotted line—jet axis.

decay rate of the turbulence. By means of these models, the Lighthill integrals can be evaluated and the sound field calculated. However the inhomogeneous, anisotropic structure of the flow is not thus taken into account. This structure is manifest in a variety of the turbulence characteristics, and these must be included in the said correlation functions if their influence on the resultant sound field is to be assessed.
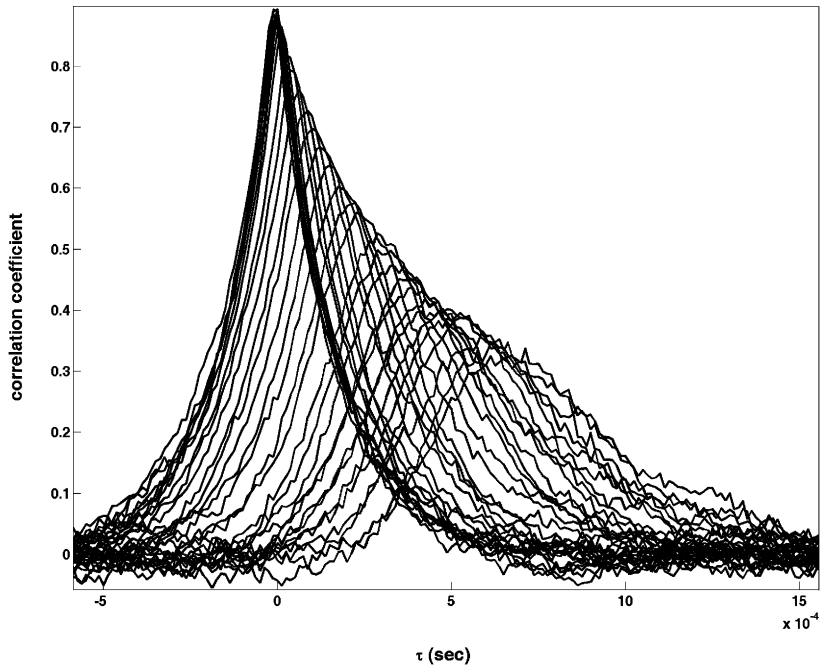
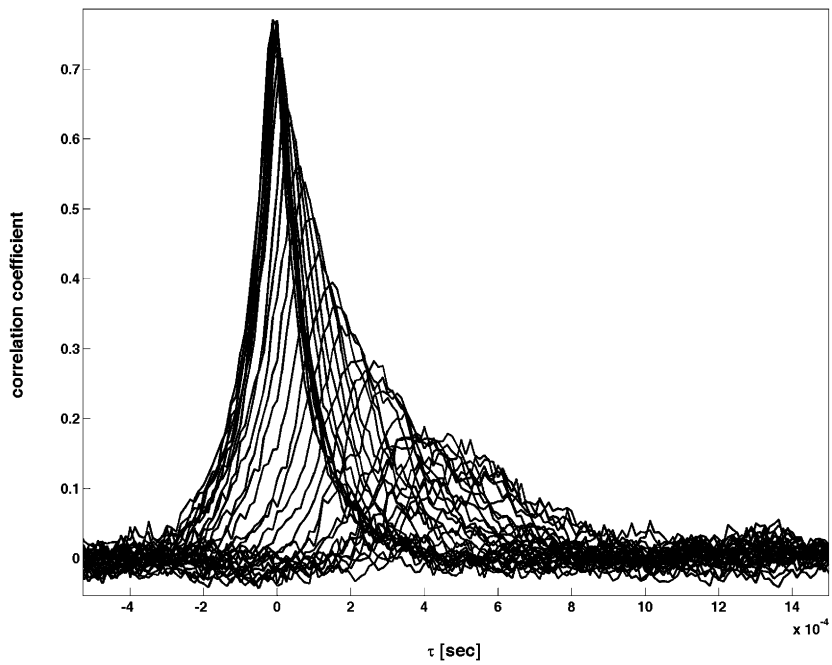Fig. 6. Two-point correlation of the axial turbulence velocity component.

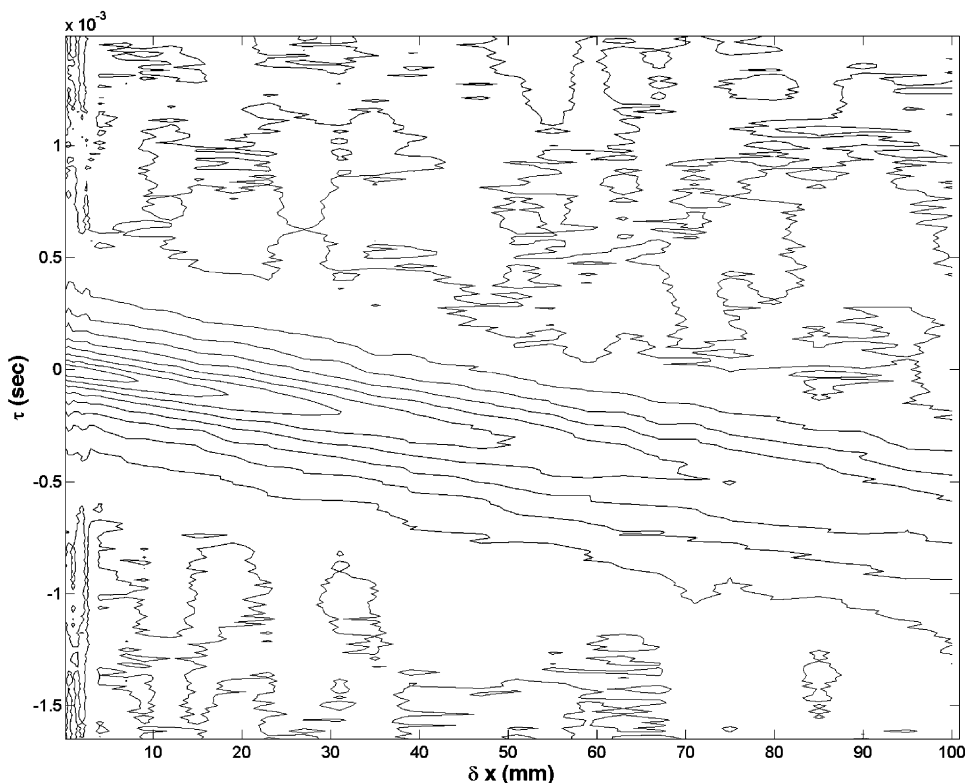Fig. 7. Two-point correlation of the axial Reynolds stress component.

Fig. 8. Two-point correlation of the axial turbulence velocity component.

4.1. Inhomogeneity

The inhomogeneity of the flow is manifest in the structure of the Reynolds stress field, as illustrated by Fig. 3. Here, the radial profiles show distributions which are approximately Gaussian, for both the axial and radial normal components uu and vv and the lateral component uv, maxima appearing on the mixing layer axis. Furthermore it can be seen that the axial component is largely dominant, demonstrating the anisotropic nature of the flow. Therefore, rather than using a single characteristic turbulence intensity as is the case in isotropic homogeneous models, each quadrupole component must include turbulence intensities corresponding to the velocity components involved. Devenport [4] has shown how this can be achieved through a modification of the expression for the homogeneous vector-potential correlation,

$$q_{ij}(\mathbf{r}, \mathbf{r}') = -\frac{u^2}{2} h(r) \delta_{ij}. \tag{8}$$

The modification involves replacing the turbulence intensity, u, with the scaling function

$$a_{ij}(\mathbf{r}, \mathbf{r}') = \tfrac{1}{2} [\tau_{ij}(\mathbf{r}) - \tfrac{1}{2} \delta_{ij} \tau_{pp}(\mathbf{r}) + \tau_{ij}(\mathbf{r}') - \tfrac{1}{2} \delta_{ij} \tau_{pp}(\mathbf{r}')], \tag{9}$$
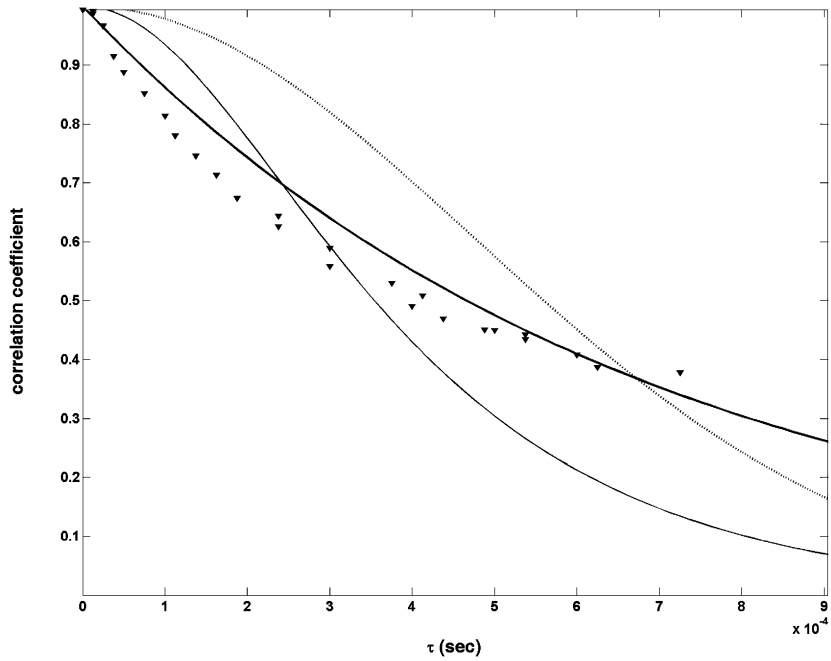
Fig. 9. Experimental and analytic moving frame temporal velocity correlation functions: ▼, experimental data; thick solid line, exponential function; thin solid line, hyperbolic function; dotted line, Gaussian function.
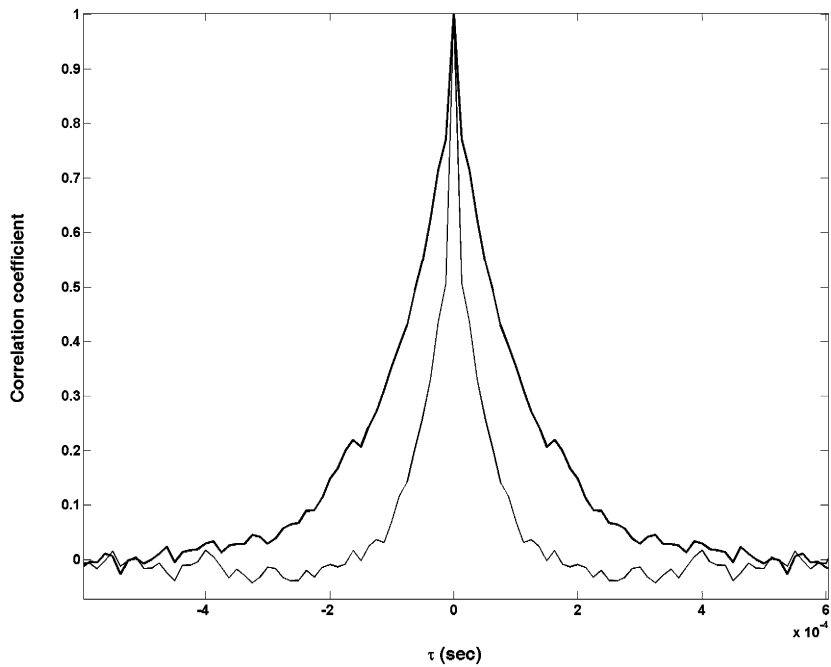

Fig. 10. Axial and radial turbulence velocity autocorrelation functions: thick solid line, axial velocity; thin solid line, radial velocity.
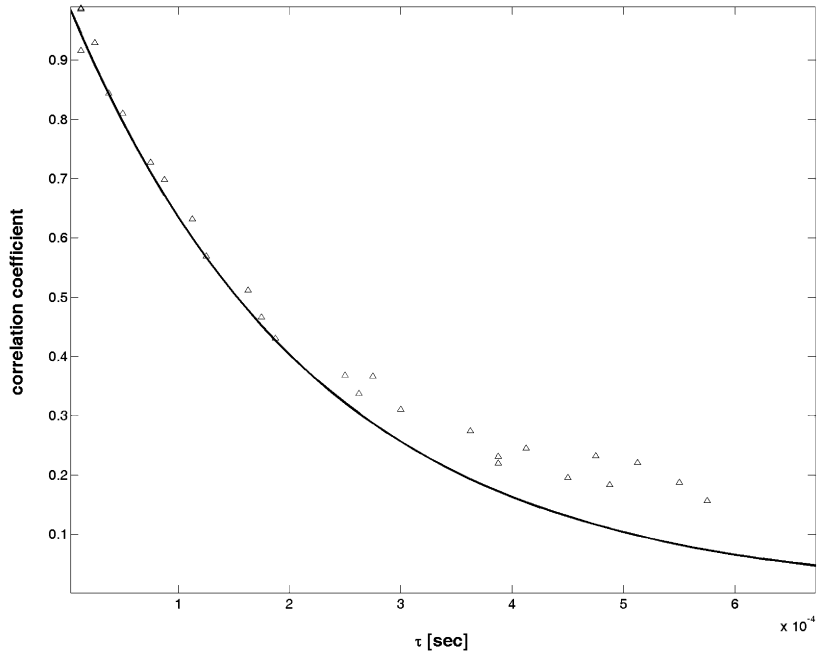
Fig. 11. Experimental (triangles) and analytic (solid line) moving frame temporal Reynolds stress correlation functions.
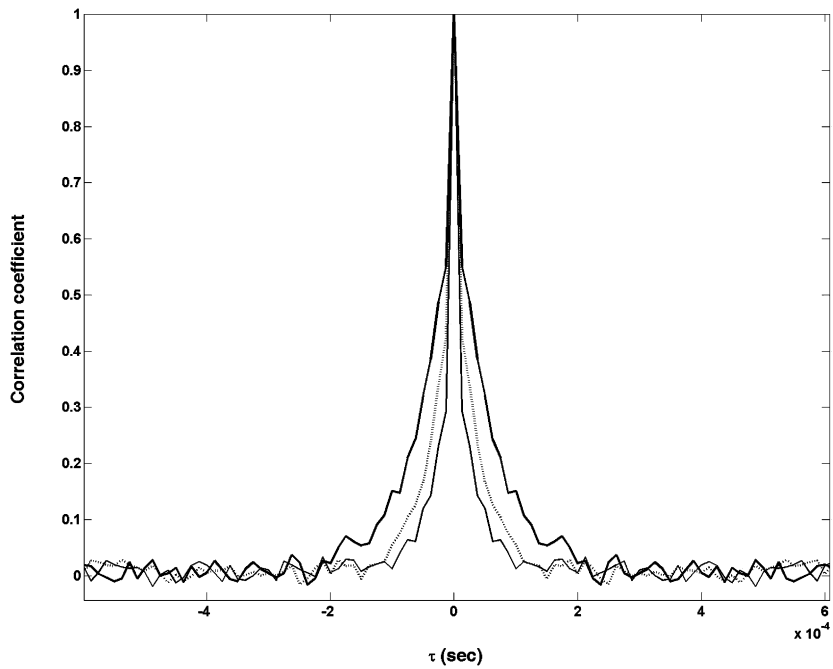

Fig. 12. Axial, radial and lateral Reynolds stress autocorrelation functions: thick solid line, axial Reynolds stress; thin solid line, radial Reynolds stress; dotted line, lateral Reynolds stress.

derived from the Reynolds stress field (see Ref. [4] for details), where τ_{ij} defines the ij tensor component, τ_{pp} is the tensor trace, and $h(r)$ ($r = |\mathbf{r} - \mathbf{r}'|$) the first moment of the longitudinal correlation coefficient function, $f(r)$, defined by

$$h(r) = \int_0^r r'f(r')\,\mathrm{d}r'. \tag{10}$$

The vector potential correlation is thus written

$$q_{ij}(\mathbf{r}, \mathbf{r}') = a_{ij}(\mathbf{r}, \mathbf{r}')h(r). \tag{11}$$

For incompressible flow the second order velocity correlation tensor can be written as the double curl of the vector-potential correlation:

$$R_{ij}(\mathbf{r}, \mathbf{r}') = \varepsilon_{ikl}\varepsilon_{jmn}\frac{\partial^2 q_{ln}(\mathbf{r}, \mathbf{r}')}{\partial x'_m \partial x'_k}. \tag{12}$$

Provided then with analytical expressions describing the structure of the Reynolds stress field and the longitudinal correlation coefficient function, this expression can be used to derive expressions for the two-point, second order velocity correlation tensor components, which include the spatial inhomogeneity of the flow.

4.2. Anisotropy

The anisotropy of the flow is manifest in the ratio of axial-to-radial turbulence intensities and integral space and time scales. The turbulence intensities have already been accounted for by Eq. (9); it remains therefore to introduce the integral scales of the flow.

4.2.1. Integral space scales

Due to the spatial anisotropy of the turbulence the rate of spatial decay is a function of direction, decaying more rapidly in the radial direction than in the axial direction. In order to account for the flow anisotropy the Gaussian function $f(r)$ is written as

$$f(r) = \mathrm{e}^{-(r^2/L^2(L_1,L_2,L_3,r_1,r_2,r_3))} \tag{13}$$

with

$$L(L_1, L_2, L_3, r_1, r_2, r_3) = \sqrt{\frac{L_1^2 L_2^2 L_3^2 (r_1^2 + r_2^2 + r_3^2)}{L_2^2 L_3^2 r_1^2 + L_1^2 L_3^2 r_2^2 + L_1^2 L_2^2 r_3^2}}, \tag{14}$$

where L_i are integral scales of the velocity field. The spatial decay of the longitudinal velocity correlation function is thus described by an ellipsoid, the major and minor axes of which are defined by the integral scales of the turbulence.

By substituting Eqs. (13) and (14) into Eqs. (10) and (12) an expression for the second order velocity correlation function is obtained in which both the Reynolds stress field and the integral space scales appear, modelling thus the anisotropic, inhomogeneous character of the flow.

4.2.2. Integral time scales

Of the various analytical forms possible for representation of the moving-frame temporal correlation, the function found to most faithfully reproduce the characteristics measured

experimentally, as seen in Fig. 9, is an exponential of the form

$$g(\tau) = e^{-|\tau|/\tau_c}, \tag{15}$$

where τ_c is the integral time scale. However as with the spatial correlation functions, flow anisotropy is not taken into account if a single time scale is used. From a series of two-component, single-point LDV measurements, autocorrelation functions of the axial and radial turbulence velocity components were determined and the anisotropy of the flow structure found to be manifest in the ratio of axial to radial time scales (obtained by integrating the correlation functions). This can be seen in Fig. 10, where the ratio of axial to radial time scale is of the order of 2. The implication here is that consideration of a single characteristic time scale to model the flow dynamic constitutes an oversimplification of the physical mechanisms involved. The existence of different scales for the different components of the turbulence illustrates how the flow dynamic is in fact more complex than this.

Time scales must thus be evaluated for both Reynolds stress and velocity fields, such that all components of both the self- and shear-noise mechanisms can be modelled. Moving and fixed frame temporal correlation functions for the Reynolds stress field are shown in Figs. 11 and 12. From the moving frame correlation functions the integral time scale of the axial component of the Reynolds stress field can be determined, while the fixed frame measurements are used to determine the ratio of axial to radial ($u^2u^2 : v^2v^2$) and axial to lateral ($u^2u^2 : u^2v^2$) scales. Six values of τ_c (corresponding to four self-noise and two shear-noise mechanisms) are thus determined and used in Eq. (15) so that the temporal character of the source components can be individually modelled.

4.3. Kelvin–Helmholtz instability

Something which none of the aforesaid correlation function models include is the Kelvin–Helmholtz (KH) instability of the jet. This instability is often associated with the passage of large coherent structures, considered important generators of sound (see Refs. [6,7] for theoretical and experimental evaluations of noise generation by large-scale structures in jets). In order to model this behaviour, a cosine term has been introduced to the temporal correlation function, such that the model will reproduce the underlying wavelike structure of the jet. The frequency used in the cosine term is the frequency of the KH instability in the case of the shear noise (modified to its value in the mobile reference frame), while for the self-noise it takes on twice this value (the self-noise has quartic dependence on the turbulence velocity while the shear-noise dependence is quadratic).

The temporal correlation function used is thus

$$g(\tau) = \cos(\omega_s\tau)e^{-|\tau|/\tau_c}. \tag{16}$$

4.4. Frequency dependence

The frequency dependence of the sound field generated by each of the source mechanism components is obtained from the cosine transform

$$G(\omega) = \int_{-\infty}^{\infty}\left[\frac{\partial^4}{\partial\tau^4}g(\tau)\right]\cos\omega\tau\,d\tau, \tag{17}$$

which after four differentiations and an integration with respect to τ gives

$$G(\omega) = -\left(\frac{\tau_c}{1 + \tau_c^2(\omega_s - \omega)^2} + \frac{\tau_c}{1 + \tau_c^2(\omega_s + \omega)^2}\right)\omega^4 + \frac{2}{\tau_c}\omega^2 - \frac{2}{\tau_c^3} + \frac{6\omega_s^2}{\tau_c}, \tag{18}$$

where insertion of the appropriate time scales and Strouhal frequencies is required for evaluation of the spectral character of the different source mechanisms.

5. Evaluation of the shear- and self-noise mechanisms

The dynamic of the constituent shear- and self-noise components can be accessed through evaluation of the second and fourth order two-point velocity correlation tensors.

5.1. Calculating the second order tensor

Calculation of the second order tensor can be effected using Eq. (7), as discussed earlier, provided expressions are available for the Reynolds stress field and the longitudinal correlation coefficient function. Radial profiles of the Reynolds stress were measured at axial positions of $x/D = 1$, 2.5 and 5. These measurements reveal Gaussian profiles for all measured components of the Reynolds stress tensor (see Fig. 3). Thus, by virtue of the self-similar evolution of the Reynolds stress field, described by the coordinate $\eta = (\sqrt{(y^2 + z^2)} - D/2)/x$, a_{ij} can be written as

$$a_{ii} = \frac{\tau_{ii}^m - \tau_{jj}^m - \tau_{kk}^m}{4}(e^{-200\eta^2} + e^{-200\eta'^2}) \tag{19}$$

for the normal components, and

$$a_{ij} = \frac{\tau_{ij}^m}{2}(e^{-200\eta^2} + e^{-200\eta'^2}) \tag{20}$$

for the off-diagonal terms. A normalized example of this is shown in Fig. 13 for $z = 0$ (i.e., a two-dimensional slice through the jet).
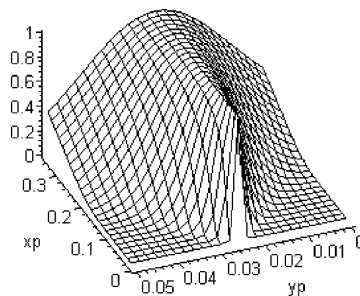

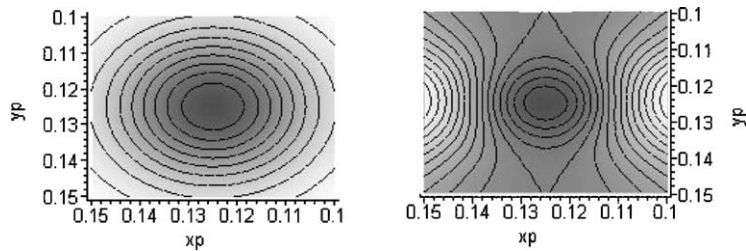Fig. 13. Self-similar evolution of the Reynolds stress field.

Fig. 14. First moment of the longitudinal correlation coefficient function, left hand plot—isotropic, right hand plot—anisotropic. Lighter shading indicates higher values.

Substituting Eq. (13) into Eq. (10) with L defined by Eq. (14) gives for the first moment of the longitudinal correlation coefficient function

$$h(L_1, L_2, L_3, r_1, r_2, r_3) = \frac{L_1^2 L_2^2 L_3^2 (r_1^2 + r_2^2 + r_3^2)}{2(L_2^2 L_3^2 r_1^2 + L_1^2 L_3^2 r_2^2 + L_1^2 L_2^3 r_3^2)} \left[1 - e^{-\frac{L_2^2 L_3^2 r_1^2 + L_1^2 L_3^2 r_2^2 + L_1^2 L_2^2 r_3^3}{L_1^2 L_2^2 L_3^3}} \right], \qquad (21)$$

a two-dimensional (xy) representation of which is shown in Fig. 14 for isotropic and anisotropic (anisotropy factor = 2) flows.

It can be seen that due to the directional spatial decay of the longitudinal velocity correlation in anisotropic flow, both the maximum value of $h(r)$ and the rate at which this value is attained are a function of space, whereas in the isotropic case both are independent of direction in the flow.[2]

Substituting Eqs. (10), (19) and (20) into Eq. (11), the vector-potential correlation can be evaluated for isotropic and anisotropic flows, whence through evaluation of Eq. (12) the second order velocity correlation tensor is obtained. Fig. 15 shows the tensor components for a two-dimensional slice (through the xy plane) for isotropic and anisotropic cases respectively. The figures show uu', uv' and vv' components of the correlation tensor where the reference position is $(xp, yp) = (0.25, 0.025)$, corresponding to the centre of the mixing layer, five nozzle diameters downstream of the jet exit.

A number of features characterise the change from isotropic to anisotropic structure. Firstly, it can be seen that there is a reduction in the characteristic dimensions (both axial and radial) of the spatial extent over which the turbulence is correlated. This is true of all three tensor components but it is most marked in the case of the uu' term. In addition to this reduction in correlation extent the uu' term shows negative "wings" in the axial direction which do not occur in the isotropic case. This characteristic is also manifest in the measured data, as shown in Fig. 16.

As Eq. (12) imposes a condition of incompressibility on the flow structure these negative wings must be compensated by additional regions of positive correlation. Four such regions are found in the R_{11} correlation (in directions of approximately 45°, 135°, 225°, and 315° relative to the correlation maximum).

---

[2] Lighter shading corresponds to higher values; xp and yp indicate axial and radial directions respectively (expressed in metres).
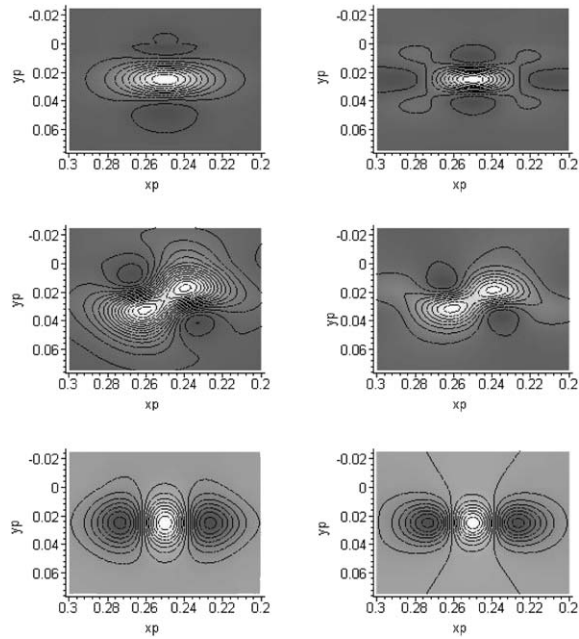
Fig. 15. Two-point velocity correlation tensor components, R_{11}, R_{12} and R_{22}—top, middle and bottom. Left hand column—isotropic, right hand column—anisotropic.
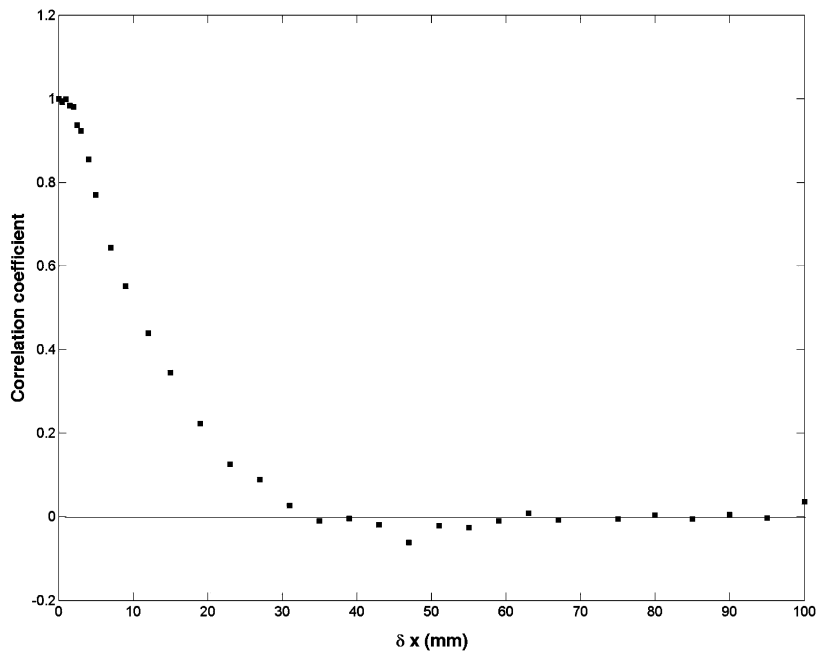

Fig. 16. Measured two-point longitudinal correlation coefficient.

5.2. Shear-noise

Having obtained an expression for the two-point velocity correlation tensor, evaluation of the integral in Eq. (6) will allow the sound production efficiency of the shear-noise source mechanism to be assessed, but for this the mean flow velocity correlation is required. This can be written

$$UU' = U_1(y_2 - r_2/2)U_1'(y_2 + r_2/2)$$

$$\simeq U_1^2(y_2) - \tfrac{1}{4}r_2^2\left[\frac{\partial U_1}{\partial y_2}\right]^2$$

and assuming a linear velocity profile

$$U_1(y_2) = -\frac{\partial U_1}{\partial y_2}r_2$$

so that

$$UU' = \frac{3r_2^2}{4}\left[\frac{\partial U_1}{\partial y_2}\right]^2. \tag{22}$$

Thus the spatial integrals for the shear-noise mechanisms become

$$\frac{3}{4}\left[\frac{\partial U_1}{\partial y_2}\right]^2\int[r_2^2 R_{11}(\mathbf{r}, \mathbf{r}')] \tag{23}$$

and

$$\frac{3}{4}\left[\frac{\partial U_1}{\partial y_2}\right]^2\int[r_2^2 R_{22}(\mathbf{r}, \mathbf{r}')]. \tag{24}$$

Fig. 17 shows graphical representations of Eqs. (23) and (24) prior to integration for isotropic and anisotropic flow structures.
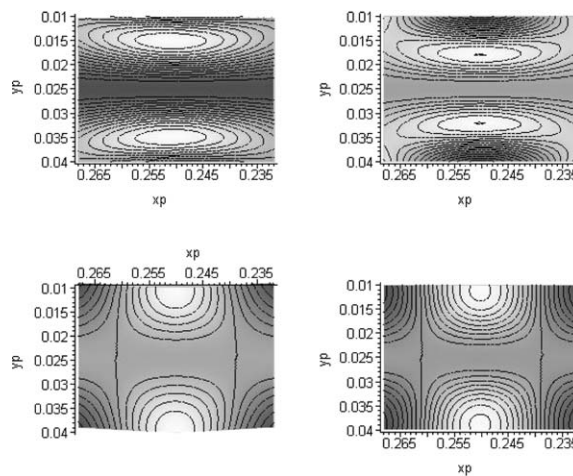

Fig. 17. Eqs. (23) and (24) prior to integration. Rows—$R11$ and $R22$ (top and bottom, respectively), columns—isotropic and anisotropic (left and right, respectively).

These forms represent the efficiency of the shear-noise mechanism. The appearance of the r_2^2 term highlights the importance of the radial dimension, as it is over this dimension that the velocity gradient exerts its influence. The greater the radial distance between two points the higher the level of shear, but only so long as those points are contained in the same correlation volume. The pair of peaks which appear in both 11 and 22 terms thus indicate those regions within a correlated volume which are most efficient in the generation of sound. The peaks are a product of the radial separation (which appears to the power of 2) between two points and the radial decay of the spatial correlation coefficient. The change from isotropy to anisotropy results in the two peaks being brought closer together, corresponding to a reduction in the spatial extent of the correlation volume. This is accompanied by globally lower levels of the correlation coefficient (not indicated in the figure), indicative of a decrease in shear-noise efficiency due to the reduced radial distance over which the velocity gradient can now exert its influence. An assumption of isotropy will therefore be likely to cause the shear-noise component of the acoustic field to be overestimated, and as the radial separation appears to the power of two, this overestimation could be expected to be substantial. This will be discussed later when self- and shear-noise efficiencies are compared.

5.3. Self-noise

Analysis of the self-noise source mechanism requires the fourth order velocity correlation tensor, which can be obtained from the second order tensor if an assumption of normal joint probability between velocity components $u_i(\mathbf{r})$ and $u_j(\mathbf{r}')$ is made (see Ref. [5]). The fourth order correlation tensor can thus be written as

$$R_{ijkl} = R_{ik}R_{jl} + R_{il}R_{jk}. \tag{25}$$

Unfortunately, this amounts to saying that the flow is homogeneous. However, having introduced inhomogeneity and anisotropy into the second order tensor, an attempt has been made to carry these qualities of the flow through to the fourth order model. As measurements were not extensive enough to allow the comparisons necessary for validation of the model, it cannot be said with certainty to what extent this has been achieved. Future work will include comparisons with the LES calculation of Andersson et al. [8] (the results of which showed excellent agreement with the measurements presented in this paper) in order to ascertain the accuracy of both second and fourth order tensor models. The results presented here are thus qualitative, being indicative nonetheless of some important differences between the mechanisms involved in the generation of shear- and self-noise.

For a two-dimensional (xy) slice through the jet, the self-noise mechanisms (fourth order correlations), 1111, 2222, 1122 and 1212 are calculated for isotropic and anisotropic flows. These are shown in Fig. 18. The change from isotropy to anisotropy can be seen to reduce the spatial extent of the correlation tensor components, although the global levels (not indicated in the figures) increase in this instance. This increase in global levels suggests that the anisotropic model may have captured some aspects of the turbulence associated with a more highly sheared flow (i.e. increased turbulence intensity). It is interesting to note that in the case of the shear-noise mechanism the change to anisotropy brought about a corresponding *reduction* in overall levels. This highlights the different nature of the two sources. The shear-noise efficiency depends more so
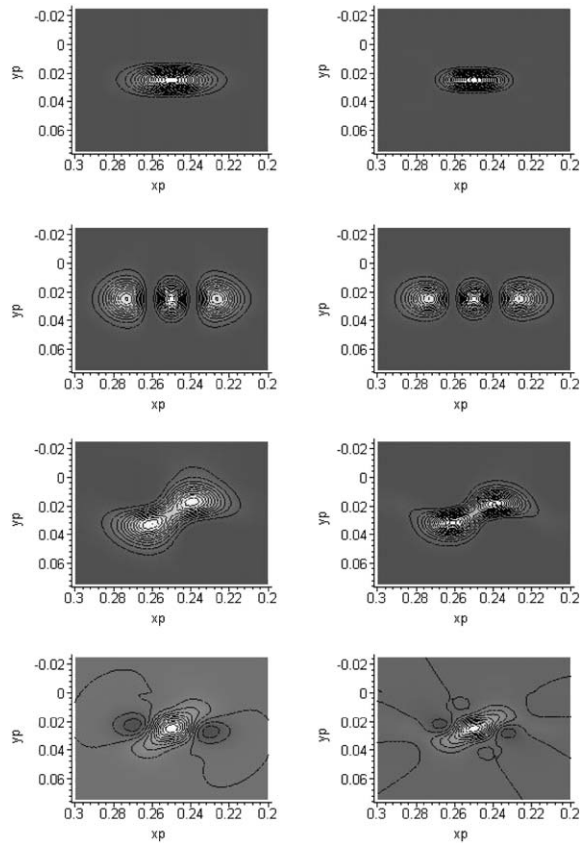
Fig. 18. Fourth order correlation tensor components, from top to bottom: 1111, 2222, 1122 and 1212 for isotropic (left hand column) and anisotropic (right hand column) flows.

Table 1
Relative self- and shear-noise component efficiencies—anisotropic assumption

	Self-noise (%)	Shear-noise (%)
1111	34	22
2222	3	8
1122	13	
1212	20	
Total	70	30

on the spatial extent of correlated regions of the flow, and in particular the radial dimension, while the self-noise is dependent rather on the intensity of the turbulence.

The relative efficiencies of the individual self- and shear-noise source components can now be estimated through evaluation of Eqs. (5) and (6). The result is summarized in Tables 1 and 2 for anisotropic and isotropic flows, respectively. The disproportionate increase in the shear-noise

Table 2
Relative self- and shear-noise component efficiencies—isotropic assumption

	Self-noise (%)	Shear-noise (%)
1111	31	41
2222	2	3
1122	9	
1212	14	
Total	56	44

levels when the flow is assumed isotropic can be seen, contributions from the axially aligned longitudinal component being almost doubled. In the anisotropic case, the self-noise is found to be the dominant source—due to the weakening of the shear noise resulting from the reduced radial extent of the correlation volumes, and in both cases the axially aligned longitudinal sources are seen to be the most significant generators of sound. The dominance of these source components means that both self- and shear-noise mechanisms are directional (the $\cos^4 \theta$ pattern dominating for both sources), which is contrary to the commonly held view (e.g., Ref. [2]) of an omnidirectional self-noise field.

5.4. The anisotropic temporal model

Through insertion of the appropriate timescales into Eq. (18) acoustic spectra are evaluated for each of the self- and shear-noise source mechanisms. These are combined with the efficiencies calculated in the previous section and the directional factors corresponding to the different quadrupole mechanisms in order to obtain the spatiospectral character of the individual source components, which when added together give the overall acoustic field. The result is presented in Figs. 19 and 20 (individual and combined fields, respectively) where the latter figure shows comparisons with the measured acoustic field.

The influence of the different integral time scales and Strouhal frequencies is manifest in the different peak emission angles and frequencies associated with the various source components.

The 1111 mechanism peaks close to the jet axis and at a frequency of about 2 kHz. The location of the peak emission angle is due to the $\cos^4 \theta$ directivity pattern associated with axially aligned longitudinal sources, while the peak frequency is a product of three factors: (1) the Strouhal frequency, (2) the axial integral time scale and (3) the Doppler shift associated with downstream radiation. In the case of the 1212 and 1122 mechanisms the peak angle is found to move slightly upstream (corresponding to a $\cos^2 \theta \sin^2 \theta$ directivity), while the spectral peak has shifted to higher frequency as a result of the smaller integral time-scale characteristic of these the lateral quadrupoles. Finally, the 2222 mechanism has a peak radiation angle characteristic of its $\sin^4 \theta$ directivity pattern (plus the convective effect), and its peak frequency results again from the three factors mentioned above, the smaller radial time scale again causing a shift towards the higher frequencies relative to the axial component. Similar characteristics are found for the acoustic fields generated by the shear-noise mechanisms.
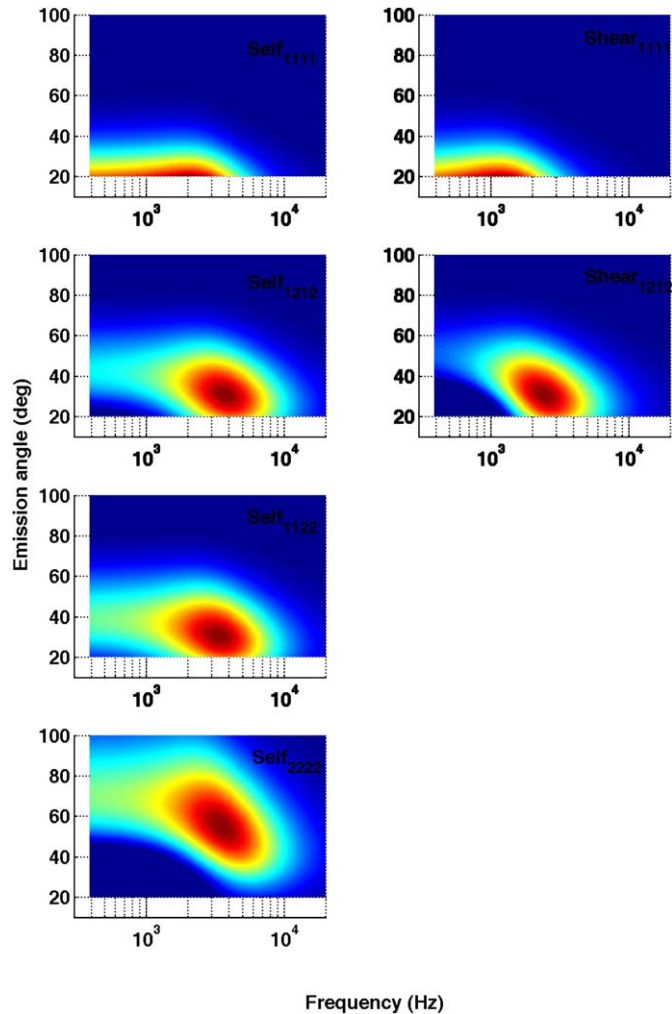
Fig. 19. Individual self- and shear-noise components with anisotropic assumption.

5.5. Comparison with acoustic measurements

5.5.1. General considerations

The overall sound field is obtained by simply adding the fields of the individual self- and shear-noise components. The result is shown in Fig. 20 where predicted acoustic spectra are shown for emission angles between $30°$ and $100°$, and compared with measurements performed at these angular stations. As the acoustic prediction is based on a single correlation volume, with time and space scales based on measurements close to the end of the potential core these results are not quantitative. The absolute levels of the calculated spectra have thus been modified for best comparison with the measured spectra.

The model shows good general agreement with the measured sound spectra. The poor agreement in the downstream direction is a result of not having taken into account the
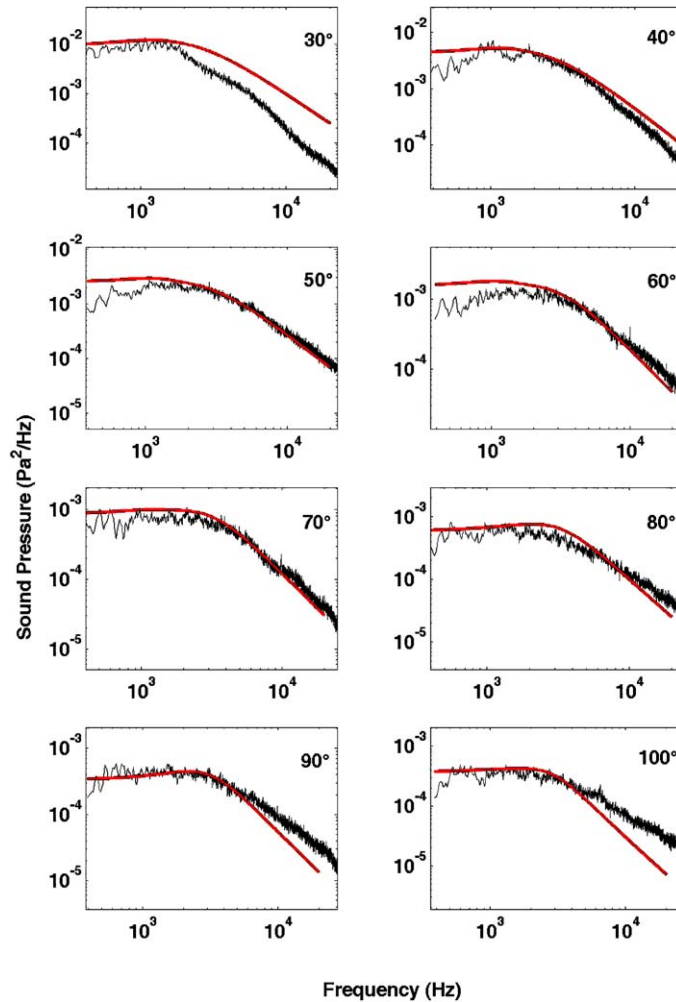
Fig. 20. Comparison of measured acoustic spectra (dashed) with anisotropic model predictions (solid).

acoustic/hydrodynamic interactions, which become increasingly significant for high frequency energy propagating in the downstream direction. The distance over which this energy has to interact with the mixing layer is comparable to or greater than its acoustic wavelength and so the influence of diffraction and refraction becomes important. The proposed model estimates the sound field as if this interaction did not occur. Inaccuracies of the broadside and upstream predictions are related to certain weaknesses of the temporal model which will be discussed later.

5.5.2. Fitting the model predictions

As the final acoustic field prediction is based on a summation of the individually calculated spectra, the relative levels of which are obtained from efficiencies evaluated using the second and fourth order velocity correlation tensor components, the flow quantities which contribute to the

final calculation are numerous. These include: the values of the 11, 12, 22, 13, 23 and 33 components of the Reynolds stresses in the centre of the mixing layer (used in Eqs. (19) and (20)), the axial and radial integral space scales of the velocity and Reynolds stress fields (used in Eq. (14) and to define the limits of integration in Eqs. (23) and (24)), the moving-frame axial and radial timescales of the velocity field and the axial, radial and lateral timescales of the Reynolds stress field (used in Eq. (18)). Of these only a small number have been measured directly, the remainder being merely estimated. For instance the timescales used were obtained from 2-pt measurements performed in the centre of the mixing layer at the end of the potential core. Timescales of 670 and 220 μs were obtained for the axial component of the velocity and Reynolds stress fields (corresponding to the 1111 shear- and self-noise mechanisms, respectively). The timescales for the other source components were then obtained using the ratio of axial to radial and axial to lateral fixed-frame timescales obtained from two-component single-point measurements.

In addition to this, calculation of the fourth order velocity correlation tensor is based on an assumption of homogeneous turbulence, and so it is likely that the self-noise efficiencies are not entirely accurate.

It is for these reasons that a number of constants were necessary to obtain a good fit of the model prediction with the measured spectra (shown in Fig. 20). These constants, used to weight the timescales in Eq. (18), took on values of 0.6, 0.6, 0.4, 0.7, 0.7 and 0.7 for the 1111_{self}, 1212_{self}, 1122_{self}, 2222_{self}, 1111_{shear} and 1212_{shear} mechanisms, respectively.

The fact that it was the time scales which were chosen as the quantities to be weighted does not necessarily imply that they are inaccurate (though this may well be the case). Rather it implies that the ensemble of values estimated for the flow quantities listed above is incorrect. Constants could alternatively have been applied to the relative source efficiencies presented in Table 1, or the Reynolds stress maxima in the mixing layer, or all of the above.

Until the said ensemble of flow quantities are directly measured it is difficult to assess the accuracy of the model. What is illustrated however, where statistical jet noise modelling is concerned, is the very large number of flow quantities and different source mechanisms implicated in the noise generation process when the assumptions of isotropy and homogeneity are dropped.

The next stage of development will involve a series of experiments aimed at measuring the said quantities for a range of jet exit conditions in order to (1) assess fully the accuracy of the model and (2) determine scaling laws such that the said quantities can be obtained by simply specifying the jet exit conditions.

5.6. Weaknesses of the temporal model

While good agreement with the measured spectra is obtained, there exist nonetheless a number of difficulties related to the choice of the temporal correlation function model. Three problems are immediately obvious. The first is manifest in the behaviour of the exponential function close to zero. The value of the first derivative of the function at $\tau = 0$ is 1 where it should be equal to 0. Thus the rapid variation of the first derivative as τ approaches zero, characteristic of the true correlation function, is not reproduced. As the final spectral prediction depends on the fourth time derivative of the exponential, the error incurred by this characteristic will be amplified, particularly in the high-frequency regime.

A second difficulty is the impossibility of independently controlling the magnitude of the instability represented by the cosine term; when the exponential decay becomes steep the influence of the cosine term becomes substantially weakened. Finally, a third difficulty is related to the un-physical nature of a monochromatic cosine term. In order to reproduce more faithfully the physics of the turbulence represented by the oscillatory part of the temporal correlation it may be better to replace this term with a truncated Fourier series, centred on the frequency of the KH instability.

These problems are no doubt the cause of some un-physical results found in the upstream predictions. The Doppler factor here causes an effective increase in the integral time scale, and the result is a spectral prediction where the high frequency regime contains almost no energy. An example is shown in Fig. 21 where a prediction at 130° is compared with a measured spectrum. An opposite effect is found when the time scale becomes too small, here the low-frequency end of the spectral model is found to approach zero.

The function is thus seen to be very sensitive to changes in the integral time scale. However it should again be noted that all but the axial moving-frame time scales used to perform these predictions were merely estimated, the estimates being based on the measured value of the latter in the mixing layer close to the end of the potential core and the radial and lateral scales measured in the fixed-frame. Integration of a more extensive range of measured scales (including those closer to the jet exit, where characteristic frequencies are higher) may improve the accuracy of these predictions.
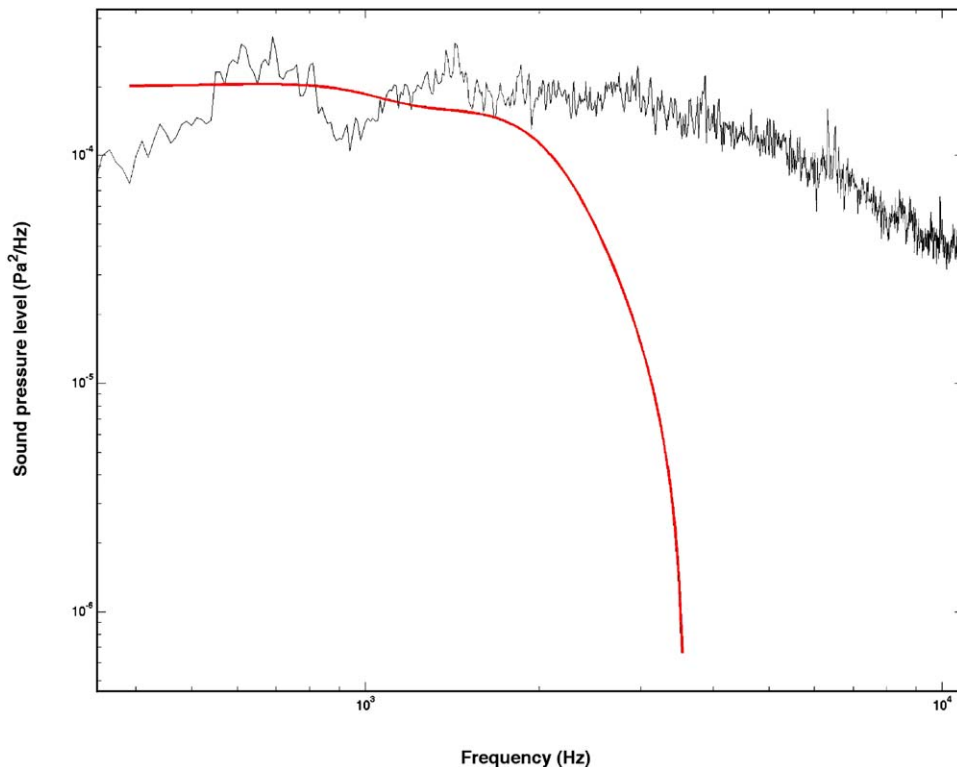

Fig. 21. Comparison of measured acoustic spectra at 130° (dashed) with anisotropic model predictions (solid).

6. Conclusion

Statistical models for the spatial and temporal correlation characteristics of inhomogeneous, anisotropic turbulence have been developed for the analysis and prediction of jet noise. Single and multi-point LDV measurements were used to supply the model with the data necessary for prediction of the acoustic fields generated by these sources. The statistical model is used to perform qualitative predictions of the noise generated by the individual quadrupoles making up the self- and shear-noise mechanisms in an isothermal jet with a Mach number of 0.75.

Results demonstrate how an isotropic assumption will lead to an overestimation of acoustic contributions from the axially aligned shear-noise quadrupoles, this being due to the role played by the radial dimension of the correlation volume. The appearance of the radial scale to the second power in the shear-noise integrals illustrates the degree to which the velocity gradient depends on this correlation dimension for its shearing effect to be efficient in the generation of sound. Another consequence of the flow anisotropy is the dominance of the axially aligned longitudinal sources, as a result of which both self- and shear-noise mechanisms are directional, the $\cos^4 \theta$ pattern being in both cases preponderant. Finally, when the flow is considered anisotropic the self-noise quadrupoles are found to dominate the shear by a factor of about 2.5.

Predictions of the spectral character of the acoustic field, as a function of emission angle, are compared with acoustic measurements made at 30 diameters from the jet. Results show good agreement for emission angles between $30°$ and $100°$. As many of the flow parameters necessary for implementation of the model were not here measured directly, they had to be estimated, and as a result a number of constants were required to obtain good agreement between the predicted and measured acoustic spectra. Direct measurement of these quantities should improve the accuracy of the model however, such that these constants are no longer necessary.

Further work will therefore include:

- direct measurement of the flow quantities used by the model,
- determination of scaling laws for prediction of these flow quantities,
- extension of the model to three dimensions and inclusion of turbulence scales from a more extensive spatial range,
- integration over the entire source volume for quantitative estimation of the jet noise,
- development of the spatial longitudinal and temporal correlation function models to more accurately represent the flow physics (see Ref. [9]),
- comparison with an LES calculation [8] to assess/improve the accuracy of the model.

References

[1] M.J. Lighthill, On sound generated aerodynamically I, *Proceedings of the Royal Society A* 211 (1952) 564–587.

[2] H.S. Ribner, Quadrupole correlations governing jet noise, *Journal of Fluid Mechanics* 38 (1969) 1–24.

[3] N. Héron, M. Ravachol, S. Candel, C. Bailly, Hot-jet-noise predictions from statistical source models, *Eighth AIAA/CEAS Aeroacoustics Conference*, Breckenridge, CO, 17–19 June 2002, AIAA, New York, 2002, p. 2003–2453.

[4] W. Devenport, C. Muthanna, R. Ma, Two-point descriptions of wake turbulence with application to noise prediction, *American Institute of Aeronautics and Astronautics Journal* 39 (2001) 2302–2307.

[5] G.K. Batchelor, *The Theory of Homogeneous Turbulence*, Cambridge University Press, Cambridge, 1953.

[6] J.E. Ffowcs Williams, The noise from the large scale structure of a jet, *Journal of Fluid Mechanics* 84 (1978) 673–694.

[7] J. Hileman, B. Thurow, Mo Samimy, An experimental effort on the connection of turbulence structures to far-field acoustic radiation in a mach 1.3 jet, AIAA Paper, May 28–30, 2001.

[8] N. Andersson, L.E. Eriksson, L. Davidson, Large-eddy simulation of a mach 0.75 jet, *Nineth AIAA/CEAS Aeroacoustics Conference*, Hilton Head, SC, 12–14 May 2003, AIAA, New York, 2003, pp. 2003–3312.

[9] F. Kerhervé, P. Jordan, Y. Gervais, J.C. Valière, Aerodynamic characterisation of a supersonic jet using two-point laser Doppler velocimetry, *Nineth AIAA/CEAS Aeroacoustics Conference*, Hilton Head, SC, 12–14 May 2003, AIAA, New York, 2003, pp. 2003–3215.